 doi:10.20944/preprints201805.0268.v1

Article

Relating Catalytic Activity of Cr/HZSM-5 in Oxidative Dehydrogenation of Liquefied Petroleum Gas under External DC Electric Field to the Fermi Level Position and Electrical Properties

Amin Alamdari [1], and Ramin Karimzadeh [2,*]

[1] Department of Chemical Engineering, Tarbiat Modares University (TMU), Jalal Al Ahmad Highway, P.O. Box 14155-4838, Tehran, Iran; amin.alamdari@modares.ac.ir
[2] Department of Chemical Engineering, Tarbiat Modares University (TMU), Jalal Al Ahmad Highway, P.O. Box 14155-4838, Tehran, Iran; ramin@modares.ac.ir
* Correspondence: ramin@modares.ac.ir; Tel.: +98 21 82883315

Abstract: CrHZSM-5 was placed in an electric field with appropriate strength in a quartz packed bed reactor with CO_2 as oxidant to analyze its catalytic activity. Olefin yield increases with decrease in band gap since lattice oxygen mobility increases by reducing band gap. Fermi level change at the catalyst surface affects the catalytic activity. One way to change Fermi level is use electric field. In high voltage electric field, energy band was curved, bending of the energy band promoted the activity and Fermi level position is increasing. The CCD experiments were carried out with Design-Expert 7.3 software to determine the interaction between four operating variables, namely: temperature, electrical current, gap distance and metal loading. The levels of the independent variables were: temperature (550-700 °C), electrical current (0-12 mA), gap distance (6-14 mm), metal loading (0.5-7.5 %wt.). The conversion of LPG (Liquefied petroleum gas) was greatly increased by weak and effective application of an electric field to the catalyst bed. The obtained results indicated that the maximum yield value (46.94%) can be achieved under 673.66 °C, input electrical current of 11.01 mA, gap distance of 6.55 mm and metal loading of 3.98 wt.%.

Keywords: electric field; oxidative dehydrogenation; LPG, Cr-/HZSM-5; electrical properties

1. Introduction

Ethylene and propylene are the most commodity chemical intermediate in petrochemical industry, which are used as feedstock for many chemicals and polymers such as plastics, rubbers, fuel blending agents and other chemicals [1-3]. Olefins are produced from reforming of natural gas, naphtha cracking and FCC processes that these methods require expensive separation stages and more purification for obtaining products [4]. Olefins are produced further in thermal cracking with steam and dehydrogenation [5-9], but, demand for olefins, environmental and economic problems for processes with nitrogen and sulfur as their feeds, researchers draw attention to economic and cleaner processes based on direct production the alkenes from alkanes. Oxidative dehydrogenation of paraffin is an appropriate alternative for old approaches of dehydrogenation in olefins production [4,10]. Now, crude source of these processes is restricted and it is required for more accessible and economical sources. Nevertheless, consideration is given to the transformation of paraffin due to increased cost of previous common feeds [11]. Also, Oxidative dehydrogenation of ethane is an appropriate alternative for highly endothermic thermal cracking process which is performed under temperature ranged from 623 K to 1273 K in isothermal or auto thermal in fixed bed, fluidized bed, monolith or membrane reactors [12]. As mentioned before, oxidative dehydrogenation of LPG is an appropriate alternative to common ethylene production process. Oxidative dehydrogenation, unlike dehydrogenation of ethane that is an endothermic process and requires high energy [6-8], is an

 doi:10.20944/preprints201805.0268.v1

exothermic process and it is an advantage of this process [10,13]. Also, thermodynamic restriction is vanishing due to the presence of oxidant and bring out hydrogen as water [6,14-15]. In addition to above advantages, the coke production is decreasing because of the presence of oxidant in oxidative dehydrogenation [7,13,16,17]. Oxidative dehydrogenation of ethane was performed in zeolite catalyst containing In, Cr, Ga, Co and Mn with oxidant CO_2. Among the aforementioned catalysts, the chromium catalysts are more common because chrome species are dispersed on the support with high specific surface area [18]. Zeolite support with metal oxides in dehydrogenation with carbon dioxide is effective but still are unstable [19]. The effect of electric properties in catalytic reaction was identified, for the first time, by Wolkenstein [20]. The fermi level influences the adsorption and electric properties of catalyst. To change fermi level, loading of multivalent metal, and exposing the catalyst under the external electric field, already are suggested. Wolkenstein studied the role of external electric field on gas adsorption on the catalyst. The external electric field changes catalytic activity. The oxidation of carbon monoxide to carbon dioxide on NiO catalyst in the presence of electric field was studied [21]. Most chemical reactions need high amount of energy to activate reagents. In these reaction, there are a few issues, including low lifetime of catalyst and heat loss problems. Heat dissipation of chemical processes is the reason for decline in their overall energy efficiency [22]. Disequilibrium hybrid plasma process is a process that uses electrons instead of heat to activate the molecules of reactant. So, expect new features such as low reaction temperatures and higher conversions rather than the existing catalytic reactions to be provided [22]. Although catalytic reactions, such as dense plasma in an electric field and a high-voltage electric field, are studied using different approaches, due to high electric power consumption, they are less efficient in term of energy. Catalytic decomposition of ethanol in an electric field was studied by Sekine et al [22]. In this research, by employing electric field, temperatures and higher catalytic activity than conventional reactions were obtained. At steam reforming of methane, $Ce_xZr_{1-x}O_2$ placed in external DC electric field at 423 K, which is hardly a typical reaction [23]. Methane conversion was significantly promoted by applying low intensity electric field on the catalyst bed. In $Ce_xZr_{1-x}O_2$ catalysts that its support promoted with electro reforming, oxygen of $Ce_xZr_{1-x}O_2$ network plays a crucial effect. Also, yield of energy for electro reforming, mechanism of reaction and effect of oxygen have been reported. Methane steam reforming is strongly endothermic and needs high temperatures. Methane oxidative coupling with CO_2 in electric field with La-ZrO_2 at 423 K was studied by Oshima et al [24]. Oxidative coupling of methane using carbon dioxide was carried out with catalysts based on La and Zr in an external electric field at a temperature of 423 K. Development in catalytic activities, rather than conventional mode, was obtained with 10 mole percent La doped in ZrO_2 in an electric field. Although catalytic activity of the catalyst for the reaction of La-ZrO_2 at 1173 K can be achieved without using an electric field. Oshima et al. (2013) [25] performed the catalytic low temperature reverse water gas shift reaction with using an electric field at 423 K. A Pt catalyst supported on La substitution in zirconium oxide (Pt/La-ZrO_2) showed high efficiency (40% ca) for reverse water gas shift reaction in the presence of external electric field at low temperature. Catalytic steam reforming of methane to produce hydrogen at low temperature in an electric field was studied by Oshima et al., (2013). Electric steam reforming of methane investigated at 423 K. Platinum catalysts supported CeO_2, $Ce_xZr_{1-x}O_2$ solid solution and a physical mixture of CeO_2 and other insulating materials (ZrO_2, Al_2O_3 or SiO_2) were used for electroreforming. Among these catalysts, platinum catalysts support on $Ce_xZr_{1-x}O_2$ solid solution showed the most activity for electroforming at 535.1 K and methane conversion was 40.6%. The results showed that interaction between electrons and metal loaded catalyst support is important for catalytic activity in electro reforming [26]. The oxidative cracking of LPG with CO_2 as oxidant was studied in external electric field. Faradaic number was employed to study the role of external electric field on the catalytic reaction. All Faradaic number was greater than 100 that indicates the reaction performed electrocatalytically. The catalytic reaction along with electric field, decreased the coke formation and the reaction temperature about 55 °C. the external electric field led to 42.58% light olefins yield and 92.12% feed conversion at 625 °C, 12 mA and 335.07 Faradaic number [27]. Transition metal oxides are used in heterogeneous catalytic reactions in the gas phase, such as oxidation of alcohols and oxidative dehydrogenation of ethane, propane and

butane [28]. Transition metal oxides act as a semiconductor, and affects the acid-base catalyst properties by varying the concentration of carrier [29]. Since metal oxide can correct carrier concentrations, consideration is given to the addition of multivalent metals to improve activity and selectivity [30]. Experimental design used for large number of variables that affects the process. Design of experiments methodology can provide results for variable effect or combination of them with minimum number of tests [31]. One of the most widely used methods of design experiments is CCD method that provides the interaction between variables and optimal process conditions for multivariable systems [32].

In the present work, the electrical properties of catalyst are linked to the catalytic activity. Central Composite Design (CCD) was employed to study how temperature, electrical current, gap distance and metal loading influence HZSM-5 catalysts in ODH of LPG to light alkenes, such as ethylene and propylene, in the presence of CO_2 and through external electric field. Analysis of variance was employed to investigate the effect of main factors and respective interaction on the light olefins yield, LPG conversion and olefin selectivity. The relevance between catalytic performance and physicochemical properties is expressed according to the experimental data. To the best of our knowledge, no such study has been previously carried out on the application of RSM technique for optimizing oxidative dehydrogenation of LPG with CO_2 in an external electric field. XRD, SEM, BET, FTIR, UV-visible, Fermi measurement, Hall and Impedance measurements employed in catalyst characterizations.

2. Results and Discussion

2.1. Materials characterization

Figure S1 in the Supplementary Material shows the XRD analyses for different catalysts. The structures were MFI with characteristic reflections at 2θ = 8.0°, 8.9°, 23.1°, 23.4° and 24.0°. The XRD of the HZSM-5, modified HZSM-5 and NaZSM-5, show that the ion exchange and impregnation did not change the structure of zeolite and no new phase formation was occurred. No peaks associated to chromium loading were obtained from pattern. So, the chromium well distributed on the catalyst surface. SEM images of Na-ZSM-5, H-ZSM-5 and 4%wt. Cr/H-ZSM-5 catalysts are presented in Figure S2 in the Supplementary Material. Catalysts had a rod-like morphology and, after the impregnation and metal loading, the structure of the catalysts did not change from orthorhombic to monoclinic. With Cr impregnation, the particles of catalysts grew in large size and the surface areas increased. Figure S3 in the Supplementary Material shows infrared spectra for NaZSM-5, H-ZSM-5 and 4%wt. CrH-ZSM-5. FTIR spectral region of ZSM-5 catalysts include bands at 1225, 1093, 970, 550 and 450 cm^{-1} which corresponded to external asymmetrical stretching, internal asymmetrical stretching, external symmetrical stretching, double five-membered ring vibration, and T-O bending modes, respectively. Absorption bands of the three catalysts were same tend. No band was around 1398 cm^{-1}, so all of the chemisorbed ammonium ions during ion- exchange treatment were converted to protons after calcination. The bands of Cr-ZSM-5 showed significant change in frequency shift or reduction in the intensity framework. The physicochemical properties for all catalyst samples are presented in Table S1 in the Supplementary Material. HZSM-5 had 0.132 cm^3/g pore volume. HZSM-5 catalyst has the highest surface area followed by different Cr/HZSM-5.

2.2. Central composite design analysis

Central composite design for three responses of olefin yield, LPG conversion and selectivity are presented in Table 1. Olefin yield was between 13.21 % wt. to 47.41% wt., LPG conversion ranged from 37.85 % to 93.56%, and selectivity was from 24.13 % to 60.0 %. The highest olefin yield (47.41%) obtained at (T= 700 °C, I=6 mA, GD=10 mm, ML=4 %) and the lowest olefin yield (13.21%) achieved at (T= 587.5 °C, I=3 mA, GD= 12 mm, ML= 2.25%). The highest conversion (93.56%) obtained at (T= 662.5 °C, I= 9 mA, GD= 8 mm, ML= 5.75%) and the lowest conversion (37.85%) achieved at (T= 625

Preprints (www.preprints.org) | NOT PEER-REVIEWED | Posted: 21 May 2018 doi:10.20944/preprints201805.0268.v1

°C, I= 0 mA, GD= 10 mm, ML= 4%). For selectivity, the highest and the lowest values (60 %) were at (T= 625 °C, I= 0 mA, GD= 10 mm, ML= 4%) and (24.13%) at (T=587.5 °C, I= 3 mA, GD= 12 mm, ML=2.25 %), respectively. The results indicated that the responses of conversion, yield and selectivity are affected with different levels of operation parameters of temperature, electrical current, gap distance and metal loading. The relation between independent factors and responses are presented in Equation 1 to 3 below:

Table 1. Central composite design of four independent parameters

Run	Factor 1: A Temperature (°C)	Factor 2: B Electrical current (mA)	Factor 3:C Gap distance (mm)	Factor 4: D Metal loading (%wt.)	Response 1: Olefin yield (%wt.)	Response 2: Conversion (%)	Response 3: Selectivity (%)
1	662.50	9.00	12.00	2.25	40.40	75.02	53.85
2	662.50	9.00	12.00	5.75	41.12	81.42	50.51
3	625.00	6.00	10.00	4.00	27.67	64.24	43.06
4	587.50	3.00	8.00	2.25	20.38	55.48	36.73
5	587.50	3.00	12.00	2.25	13.21	54.76	24.13
6	625.00	6.00	6.00	4.00	31.13	67.53	46.10
7	662.50	3.00	12.00	2.25	34.31	65.67	52.24
8	625.00	6.00	10.00	4.00	27.35	65.46	41.78
9	587.50	9.00	8.00	5.75	32.18	78.75	40.86
10	625.00	12.00	10.00	4.00	33.86	86.04	39.35
11	625.00	6.00	14.00	4.00	27.16	64.24	42.28
12	587.50	3.00	12.00	5.75	24.13	57.50	41.97
13	587.50	9.00	12.00	2.25	28.66	62.22	46.06
14	662.50	9.00	8.00	2.25	40.63	78.77	51.59
15	587.50	9.00	12.00	5.75	31.40	67.04	46.84
16	662.50	9.00	8.00	5.75	42.20	93.56	45.10
17	662.50	3.00	8.00	5.75	38.91	72.05	54.00
18	625.00	6.00	10.00	0.50	22.59	54.28	41.63
19	625.00	6.00	10.00	7.50	33.10	71.81	46.10

Preprints (www.preprints.org) | NOT PEER-REVIEWED | Posted: 21 May 2018 doi:10.20944/preprints201805.0268.v1

20	700.00	6.00	10.00	4.00	47.41	84.42	56.16
21	625.00	0.00	10.00	4.00	22.71	37.85	60.00
22	625.00	6.00	10.00	4.00	27.85	64.24	43.35
23	625.00	6.00	10.00	4.00	28.70	64.24	44.66
24	550.00	6.00	10.00	4.00	20.50	50.33	40.73
25	625.00	6.00	10.00	4.00	28.01	64.24	43.59
26	662.50	3.00	12.00	5.75	38.26	69.16	55.32
27	587.50	9.00	8.00	2.25	30.74	63.93	48.09
28	587.50	3.00	8.00	5.75	26.45	58.56	45.18
29	625.00	6.00	10.00	4.00	27.90	64.24	43.42
30	662.50	3.00	8.00	2.25	36.45	68.90	52.90

151

$$Yield=449.05-1.50X_1+8.19X_2-9.55X_3+7.30X_4-0.01X_1X_2+0.006X_1X_3-0.01X_1X_4+0.08X_2X_3 -0.20X_2X_4+0.12X_3X_4+0.001X_1^2+0.04X_2^2+0.18X_3^2+0.17X_4^2 \quad (1)$$

$$Conversion=304.67-0.86X_1+3.76X_2-7.46X_3-6X_4+0.005X_1X_2-0.004X_1X_3+0.004X_1X_4-0.24X_2X_3 +0.31X_2X_4-0.36X_3X_4+0.0008X_1^2-0.30X_2^2+0.60X_3^2+0.95X_4^2 \quad (2)$$

$$Selectivity=249.89-0.82X_1+11.14X_2-11.21X_3+17.89X_4-0.02X_1X_2+0.017X_1X_3-0.025X_1X_4+0.34X_2X_3 -0.62X_2X_4+0.50X_3X_4+0.0008X_1^2+0.42X_2^2-0.21X_3^2-0.36X_4^2 \quad (3)$$

152 The significance of central composite model was investigated based on analysis of variance. Analysis
153 of variance for responses of this study is presented in Table S2 in the Supplementary Material. As
154 shown in Table S2 in the Supplementary Material, correlation coefficients have high values and the
155 model can predict the experimental responses with high accuracy (R^2 = 0.96 for conversion, R^2 = 0.96
156 for selectivity and R^2=0.96 for yield). Figures S4a-c in the Supplementary Material show the
157 predicted olefin yield, selectivity and LPG conversion versus the experimental results of these
158 responses and it indicated proximity between predicted value and experimental results. The
159 adjusted value of R^2 for olefin yield, selectivity and LPG conversion were 0.93, 0.96, and 0.93,
160 respectively. The adjusted value of R^2 is more suitable for accuracy of CCD model. Significance of
161 the model was studied with F-value and P-value of the model for CCD results. The higher F value
162 and lower P value show the model significance. F-value resulted for olefin yield, selectivity and LPG
163 conversion were 29.84, 31.36 and 31.66, respectively. These values were higher than Fishers F-value
164 that is 2.37% at 95% confidence limit, and it shows that the model is good for describing olefin yield,
165 selectivity and LPG conversion in oxidative dehydrogenation of LPG in an external electric field. In
166 order to achieve a simpler model and a model with better fit for each response, such as olefin yield,
167 LPG conversion and selectivity, insignificant terms with p values greater than 0.5 will be deleted
168 from CCD model. Final responses will be provided on the basis of a quadratic equation as follows:

$$Yield=449.05-1.50X_1+8.19X_2-9.55X_3+7.30X_4-0.01X_1X_2-0.20X_2X_4 \quad (4)$$

Preprints (www.preprints.org) | NOT PEER-REVIEWED | Posted: 21 May 2018 doi:10.20944/preprints201805.0268.v1

$$Conversion=304.67-0.86X_1+3.76X_2-7.46X_3-6X_4+0.31X_2X_4-0.30X_2^2+0.60X_3^2+0.95X_4^2 \quad (5)$$

$$Selectivity=249.89-0.82X_1-0.02X_1X_2+0.017X_1X_3-0.025X_1X_4+0.34X_2X_3+0.50X_3X_4+0.42X_2^2 \quad (6)$$

Coefficients of regression, standard error, F and P values are shown in Table S3 in the Supplementary Material for olefin yield, LPG conversion and selectivity respect to conversion. In a confidence limit of 95% for olefin yield, linear significant coefficients are A, B, C, D, quadratic significant coefficient is A^2, and significant interaction coefficient are AB, BD. So, the linear effect of temperature, input electrical current, gap distance and metal loading, quadratic effect of temperature and interaction effect of temperature-electrical current and electrical current-metal loading are statistically significant variables. In a confidence limit of 95% for LPG conversion, linear significant coefficients are A, B, C, D are significant model terms. Quadratic significant coefficients are A^2, B^2, C^2 and D^2, and significant interaction coefficient is BD. So, linear effect of T, I, GD and ML, quadratic effect of T, I, GD and ML and interaction effect of input electrical current-metal loading are statistically significant variables. In a confidence limit of 95%, for selectivity respect to conversion, linear significant coefficient is A, quadratic significant coefficients are A^2, B^2, C^2, D^2, and significant interaction coefficients are AB, AC, AD, BC, BD, CD. So, linear effect of T, quadratic effect of T, I, GD and ML and interaction effect of I-GD, T- GD, T-Ml, I-GD and GD- ML are statistically significant variables.

In order to evaluate the four variables with together on conversion, selectivity and yield the perturbation curve was used. The model can be used to compare the effect of main factors in design point. Figure S5 shows the perturbation curve for all three responses. Steep or curved graph indicates that the response is sensitive to main factors. Accordingly, as shown in Figure S5 in the Supplementary Material, in order to achieve maximum olefin yield and LPG conversion, temperature, electrical current and metal loading are controlling factors. Steep curvature of electrical current and temperature rather than gap distance and metal loading, revealed that the olefin yield is sensitive to these parameters. For selectivity, these parameters are fewer.

In order to study the interactive effect of these four factors on olefin yield, 3D and contour plot were shown in Figure 1, Figure 3 and Figure 5 and shown in Figure S6, Figure S7 and Figure S8 in the Supplementary Material for selectivity and LPG conversion. Response surface model diagram for different values of parameters predicted olefin yield, LPG conversion and selectivity for process parameters and interactions between process parameters. Figure 1 and Figure S6a in the Supplementary Material show contour plot and response surface for interaction between temperature and input electrical current when gap distance and metal loading were 10 mm and 4%wt, respectively for yield and conversion. As indicated, olefin production efficiency and LPG conversion increased with increase of electrical current. This could be due to resonance effect of external electric field and an electrostatic field inside the zeolite. As can be seen, increasing temperature resulted in an increase in yield (%). So, it indicates that temperature leaves a major effect on olefin yield (%). This can be confirmed with amount of F value obtained for yield. Figure S6b in the Supplementary Material shows contour plot and response surface for interaction between temperature and input electrical current, when gap distance and metal loading were 10 mm and 4%wt, respectively for selectivity. As indicated, selectivity increases with increase in temperature and decrease in electrical current.

Preprints (www.preprints.org) | NOT PEER-REVIEWED | Posted: 21 May 2018 doi:10.20944/preprints201805.0268.v1

a)

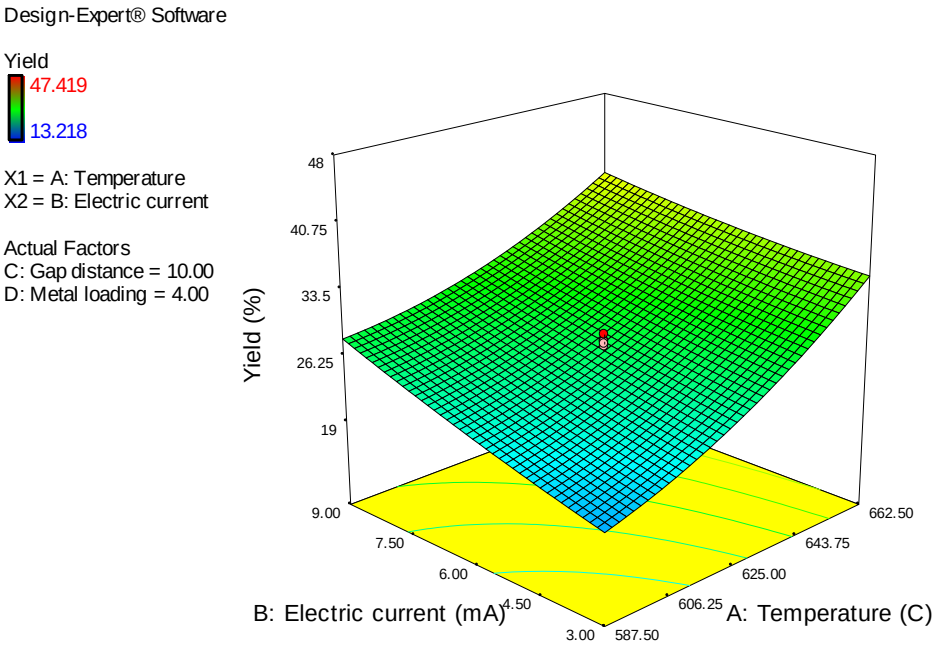

b)

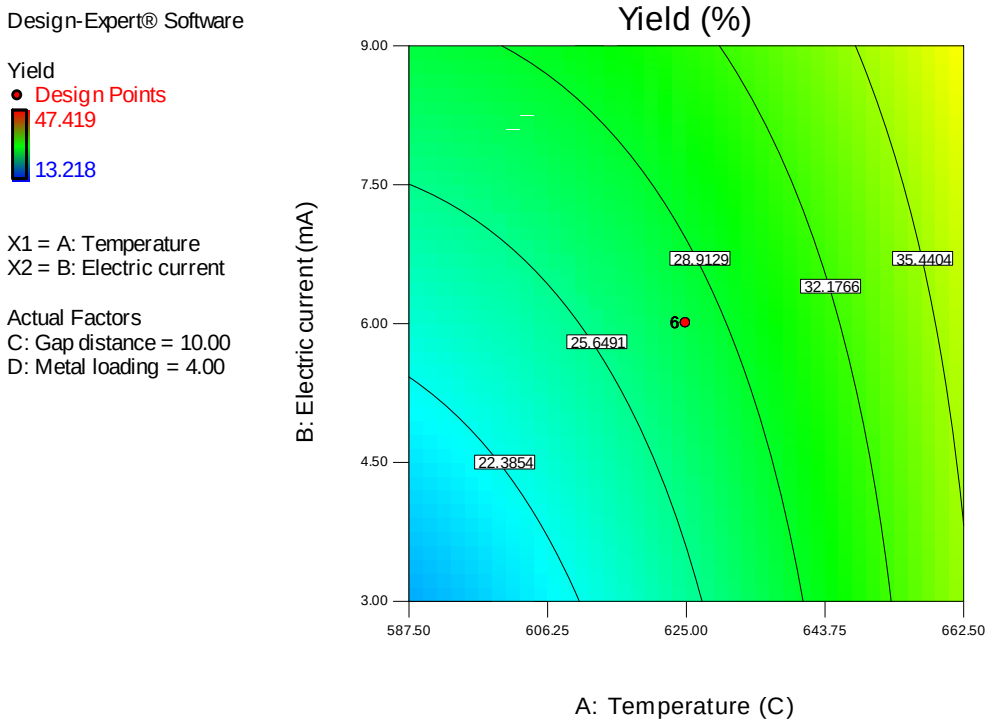

Figure 1. (a) The response surface; and (b) contour plots as a function of the temperature and electrical current whereas the gap distance and metal loading are constant at 10 mm and 4wt%, for olefin yield.

To investigate the behavior of catalytic performance of zeolite in external electric field, not only it is necessary to know the properties, chemical composition and structure of zeolite, but also the

Preprints (www.preprints.org) | NOT PEER-REVIEWED | Posted: 21 May 2018 doi:10.20944/preprints201805.0268.v1

movement of external cations. The movement of these cations is achieved by measuring electrical conductivity and dielectric constant [33].

Electrical properties of zeolite are important. The electrical properties of different ZSM-5 were studied at 100 Hz frequency with Impedance Analyzer. ZSM-5 has MFI crystalline structure. The results of electrical properties, related to the catalytic activity. Zeolites can be classified as a dielectric material. In the presence of external electric field, dielectric material stores electrical energy. Electric filed moves free electrons to ZSM-5 and equilibrium occurs after charge displacement. This process is known as displacement electronic polarization phenomena. In the electric field with intensity E, displacement can be defined as $D = \varepsilon_0\varepsilon_r E$, where, ε_0 and ε_r are free space permittivity and relative permittivity. ε_r is a complex number ($\varepsilon_r=\varepsilon'-j\varepsilon''$). Complex relative permittivity consists of two parts. The real part is $\boldsymbol{\varepsilon'}$ (permittivity) and describe the energy storage in dipolar cells. The imaginary part is $\boldsymbol{\varepsilon''}$. (dielectric loss) which is attributed to internal friction in zeolite. Permittivity is a criterion for energy storage within zeolite dipoles, and dielectric loss is a criterion for energy loss in the zeolite originated from internal friction.

To relate catalytic activity to electrical properties, these properties were investigated. To the best of our knowledge, this work is the first attempt to investigate of role of permittivity and loss factor on operation process variables including T, I, GD and ML. At first, for impedance analysis, the pellet of catalyst samples is prepared with 6.5 mm diameter and 1.2 mm thickness. Then, the samples are inserted on a ceramic plate and heated at various temperature for 1 hr. Then, samples are cooled down to 25 °C. The conductance ($G=\varepsilon''\omega C_0$) and susceptance ($B=\varepsilon'\omega C_0$) of samples are determined in frequency 100 Hz at 25 °C (ω is angular frequency). The model of Impedance Analyzer was using an HP 4194A LF. Finally, electrical properties of catalysts are calculated in the mentioned frequency range.

The effect of temperature on dielectric constant and loss factor are presented in Figure 2. The permittivity increases with increasing temperature. As shown in Figure 2a, at 700 °C, permittivity reaches its highest value. An increase in motion of carrier charge with temperature and permittivity is reported [34]. The increase in dielectric constant with temperature is due to the electric conduction, which results from the movement of ions in channels and zeolite cavities and some metal impurities in zeolite materials. Also, increase the temperature leads to increase dipole energy in zeolite materials. Dipole subjected to external electric field indicates that temperature increase leads to decrease in relaxation time of dipole.

The catalytic activity is increased with temperature under electric field with high intensity. Conductivity increases with temperature in this frequency range. Such an increase may have many reasons; increasing the charge carriers due to increased crystalline defects can cause local energy toward to the conduction or valance band energy. Metal oxide ions in zeolite structure can move positive ions, and thus, the temperature increases ion movements [35]. The loss factor is presented in Figure 2b at various temperatures. The temperature increased the loss factor. The loss factor shows the ability of zeolite to extraction of energy from external electric field. The increase in $\boldsymbol{\varepsilon'}$ and $\boldsymbol{\varepsilon''}$ is attributed to increase in mobility of charge carrier. So, at higher temperature and higher electrical current the yield and conversion increased. The a.c. conductivity is shown at different temperatures in Figure 2c. The conductivity has a direct relation with temperature. The minimum conductivity is resulted at 550 °C which can be ascribed to Zeolites contain movable and interchangeable cations. These cations form a weak bond with adjacent atoms, rather than framework ions [36]. Electrical conductivity of zeolite is affected by adsorbed molecules [37]. Electrical conductivity depends on the current carriers [38]. It is useful to know the electric conduction mechanism in processes that are affected by the external electric field. Figure 2c shows the a.c. conductivity. Cole-Cole plots of zeolite is shown in Figure 2d. The separation of loss from conductivity is confirmed by the circular arc plot. Charging of catalysts influences catalytic activity because of electron transfer from surface of catalyst to the reactants and charging increases with temperature and permittivity [39, 40].

Preprints (www.preprints.org) | NOT PEER-REVIEWED | Posted: 21 May 2018 doi:10.20944/preprints201805.0268.v1

a)

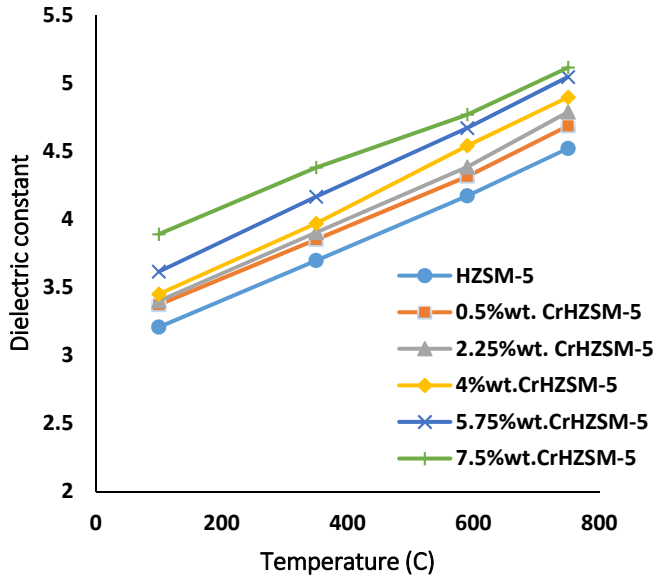

b)

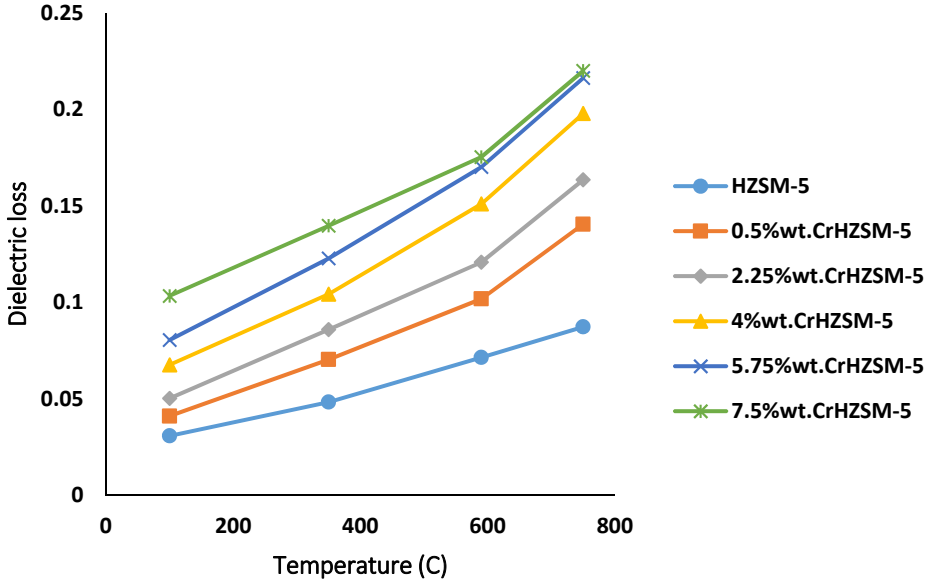

Preprints (www.preprints.org) | NOT PEER-REVIEWED | Posted: 21 May 2018 doi:10.20944/preprints201805.0268.v1

c)

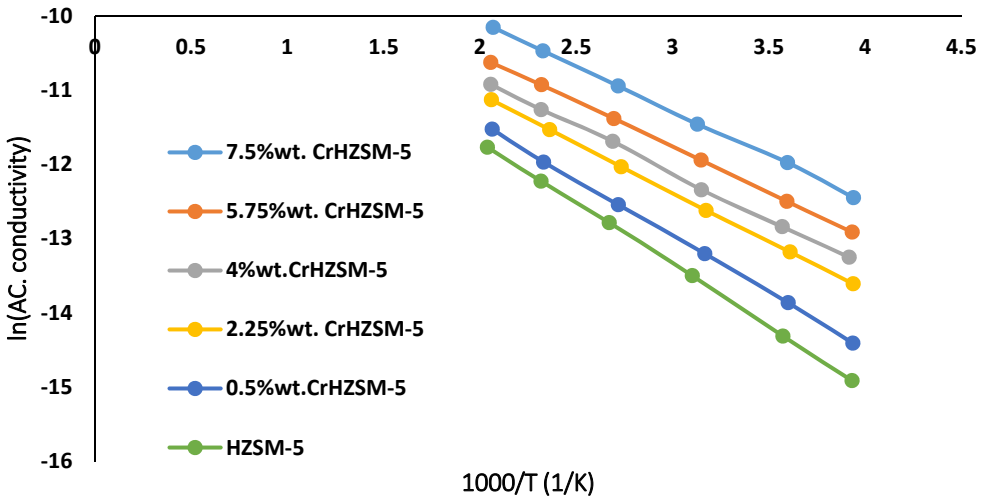

d)

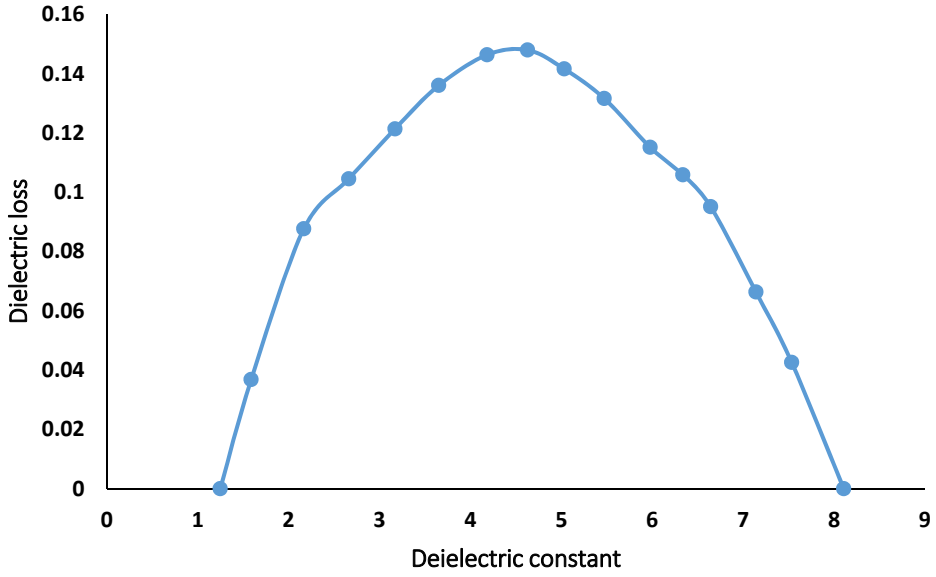

Figure 2. (a) Dielectric constant; (b) Dielectric loss; (c) Ac conductivity versus temperature for different CrHZSM-5; (d) Cole-Cole plot.

Figure 3 and Figure S7a in the Supplementary Material show contour plot and response surface for interaction between electrical current and metal loading when gap distance and temperature were 10 mm and 625 °C, respectively, for yield and conversion. As indicated, olefin yield and LPG conversion increase with increase in electrical current and metal loading. As can be seen, Simultaneously, increase in intensity of input electric current and metal loading had greater impacts on conversion. Figure S7b in the Supplementary Material shows contour plot and response surface for interaction between electrical current and metal loading, when gap distance and temperature were 10 mm and 625 °C, respectively, for selectivity. As indicated in Figure S7b in the Supplementary Material, selectivity increases with increase in electrical current and decrease in metal loading. Increase in intensity of electric current and decrease in metal loading, or vice versa, would achieve greater selectivity.

Preprints (www.preprints.org) | NOT PEER-REVIEWED | Posted: 21 May 2018 doi:10.20944/preprints201805.0268.v1

296 a)

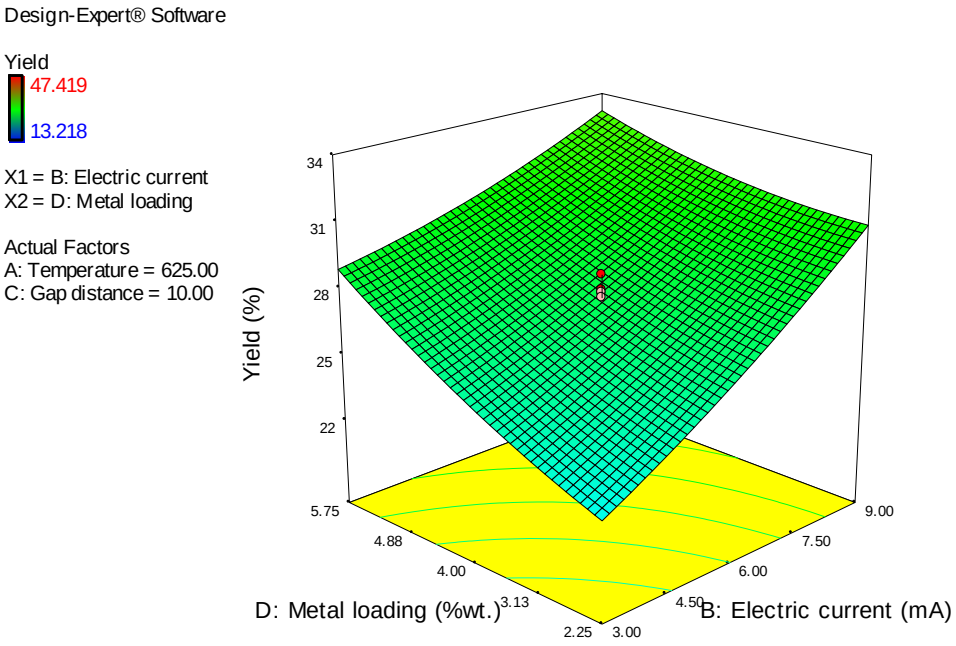

297

298 b)

299

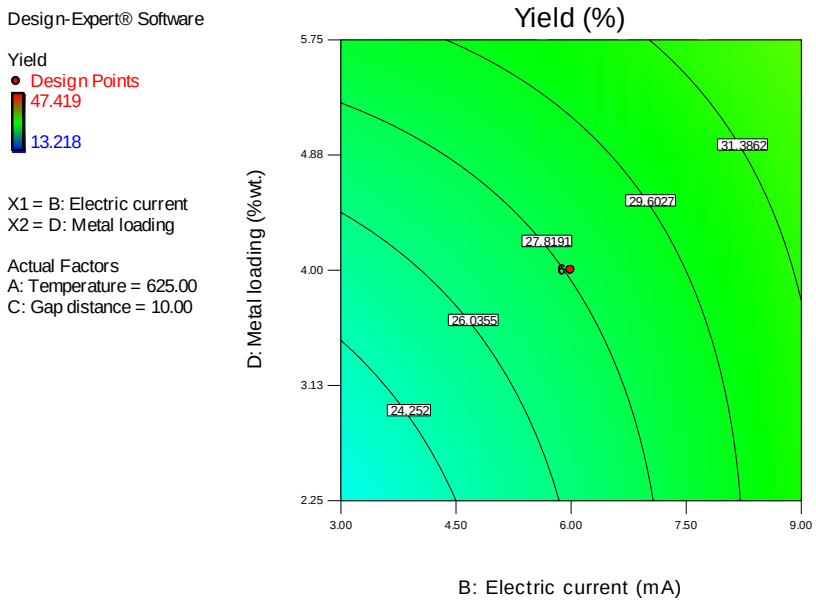

300

301 **Figure 3.** (a) response surface; and (b) contour plots as a function of the electrical current and metal
302 loading whereas the temperature and gap distance are constant at 625 °C and 10 mm, respectively for
303 olefin yield.

304 When catalytic samples are received light with a specified intensity, if the energy of absorbed
305 photons on the catalyst surface is greater than or equal to the band gap, optical transmission occurs,
306 and electrons can excite from bottom valance band to the upper conduction band. Figure 4a shows

Preprints (www.preprints.org) | NOT PEER-REVIEWED | Posted: 21 May 2018 doi:10.20944/preprints201805.0268.v1

UV-visible spectra for different ZSM-5 in the range of 200 to 1100 nm. Absorption increase with increase in wavelength. Figure 4b present F(R) versus photon energy. Extrapolation for these absorption curves leads to optical band gap. According to Table 2, band gap decreases with increasing metal loading.

There is a strong relation between band gaps, as indicator of species movement in different zeolite lattices, with olefin yield, which offers correlation between species conductivities and distribution of products. The band gaps of metal oxides relate with catalysts capability to activation of oxygen of lattice [41]. Figure 4 shows the band gap determination for HZSM-5 and different CrHZSM-5 by diffuse reflectance IR spectroscopy. Figure 4a, shows absorbance versus wavelength and Figure 4b shows F(R) versus E whose slope in Figure 4b, creates band gap. The band gap decreased with Cr impregnation and it shifts to the lower energy band. The least and the most band gap were 2.1 eV and 2.95 eV, respectively. As a result, Chromium decreases the electronic band gap. As it can be seen in Figure 4b decrease from 2.95 eV to 2.1 eV occurs when impregnation is between 0.5 wt.% to 7.5 wt.%. Activation the lattice oxygen and mobility of oxygen species of surface and lattice are important factors in determination of olefins selectivity in alkanes oxidative dehydrogenation [42]. As shown in Table 2, there is a relation between olefin yield and band gap. Olefin yield increases with decrease in band gap since lattice oxygen mobility increases by reducing band gap. This leads to higher hydrogen abstraction from ethyl and propyl species to produce olefins [43], and selectivity to olefin increased. An increase in band gap reduces diffusion rate of surface oxygen into lattice space of the different catalyst and surface adsorbed electrophilic oxygen species increases [44]. Hall coefficients (R_H) of all catalysts were positive and this indicates p-type conduction in the catalysts. The carrier concentration is reported in Table 2. Chromium acts as p-type in HZSM-5 support catalysts. By impregnating chromium, an increase in carrier concentration occurs.

Figure 2c presents dependency of electrical conductivity on temperature. At ambient temperature, the electrical conductivity increases by impregnation up to 8%wt. when the chromium metal is loaded. An increase in conductivity with chromium concentration in CrHZSM-5 is due to increase in hole concentration.

Table 2. The relation between electrical property and catalytic activity.

Catalyst	Band gap (eV)	F(eV)	$\varepsilon(-)$	$P \times 10^{20}$ (cm^{-3})	FE(eV)	Yield (%wt.)
HZSM-5	2.95	0.64	1.7	3.31	0.68	18.03
0.5 wt.% Cr/HZSM-5	2.9	0.78	2.39	3.64	0.97	22.59
2.25 wt.% Cr/HZSM-5	2.7	0.86	2.85	3.89	1.09	24.78
4 wt.% Cr/HZSM-5	2.5	0.95	3.02	4.21	1.23	28.70
5.75 wt.% Cr/HZSM-5	2.4	1.19	3.24	4.56	1.39	31.09
7.5 wt.% Cr/HZSM-5	2.1	1.35	3.56	4.85	1.78	33.10

Preprints (www.preprints.org) | NOT PEER-REVIEWED | Posted: 21 May 2018 doi:10.20944/preprints201805.0268.v1

a)

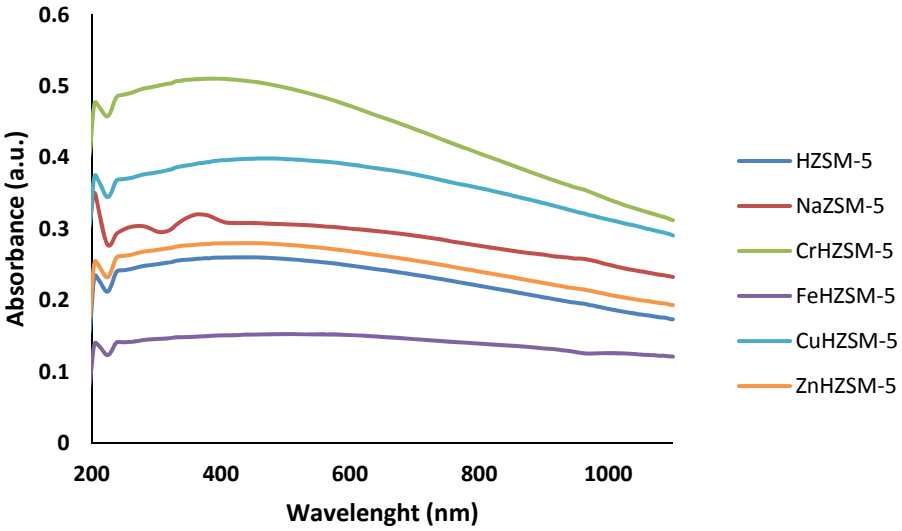

b)

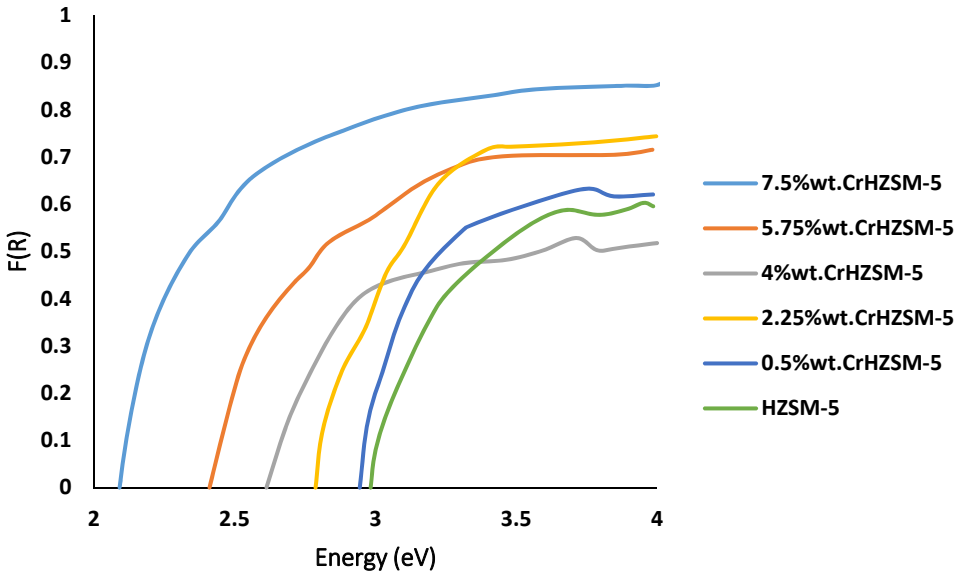

Figure 4. (a) Diffuse reflectance UV−visible absorption spectra for different catalysts; (b) Graphical of F(R) versus E for different catalysts to determine the band gap.

Figures 5 and Figure S8a in the Supplementary Material show contour plot and response surface for interaction between electrical current and gap distance, when temperature and metal loading were 625 °C and 4%wt, respectively, for yield and conversion. As indicated, olefin yield and LPG conversion increase with increase in electrical current and decrease in gap distance between two electrodes. The crucial role of input electric current is higher than gap distance. Figure S8b in the Supplementary Material shows contour plot and response surface for interaction between electrical current and gap distance when temperature and metal loading were 625 °C and 4%wt, respectively for selectivity. As indicated, selectivity increases with increase in electric current and gap distance or

Preprints (www.preprints.org) | NOT PEER-REVIEWED | Posted: 21 May 2018 doi:10.20944/preprints201805.0268.v1

reduces both, simultaneously. In the conventional reaction, yield and conversion were 22.71% and 37.85%, respectively, at T= 625 °C, GD=10 mm gap distance and ML=4%wt. metal loading, but in the 6 mA external electric field, yield and conversion were 28.79 and 64.24%, respectively, at T= 625 °C, GD=10 mm gap distance and ML=4%wt. metal loading.

a)

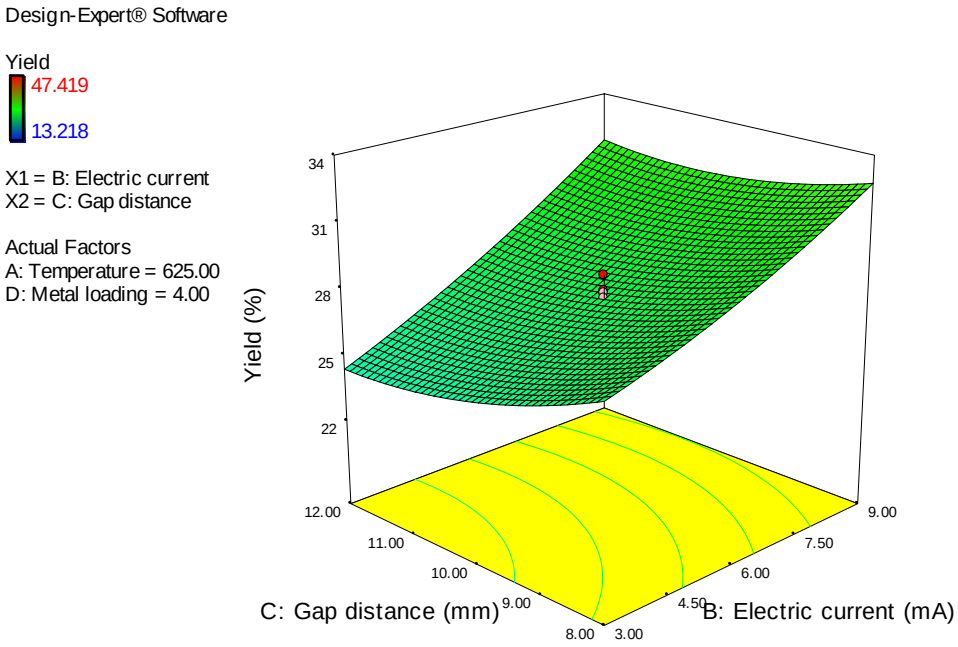

b)

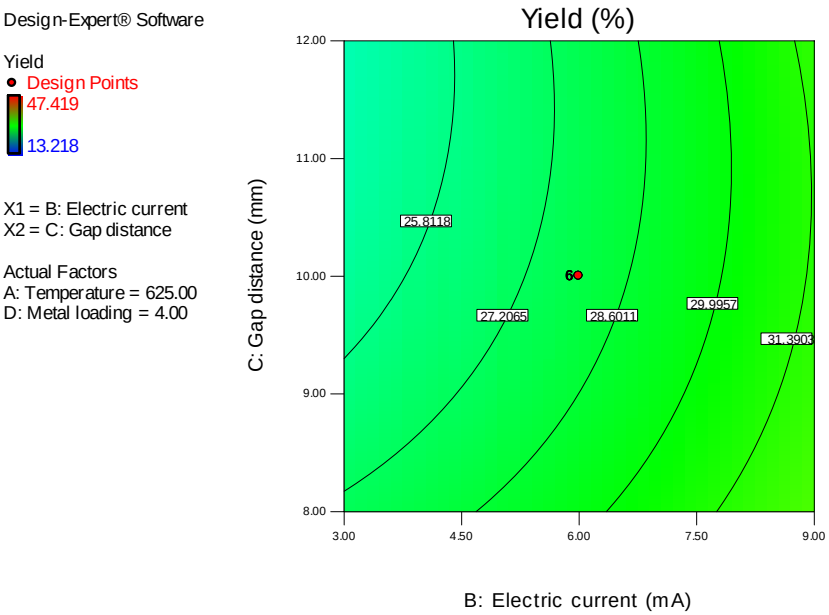

Figure 5. (a) response surface; and (b) contour plots as a function of the electrical current and gap distance whereas the temperature and metal loading are constant at 625 °C and 4%wt., respectively for olefin yield.

 doi:10.20944/preprints201805.0268.v1

Catalytic activity can relate to the Fermi level position and electrical properties. Table 2 shows the Fermi level and electrical properties for different catalysts. In external electric field, energy bands are curved and Fermi level position is changed according to Equation 7.

$$F_S(E)=F_S+V_S(E) \quad (7)$$

where, Fs(E) is location of fermi level in the presence of external electric field, E is intensity of electric field, Fs is location of fermi level in conventional reaction, and Vs(E) is bending in energy bands. By inserting catalyst in external electric field, reaction rate increases [21]; it is a character of donor process. Bending energy bands, V_s (E), is described as follow:

$$V_S(E)=ELq \quad (8)$$

where, q is elementary charge and L is Debye screening length which is determined with concentration of current carrier (p) and dielectric constant of catalyst.

$$L=\left(\frac{\varepsilon\varepsilon_0 kT}{q^2 p}\right) \quad (9)$$

where, T is temperature, k is Stefan Boltzmann constant, ε and ε_0 are permittivity of catalyst and free space, respectively. Table 2 shows Fermi level and electronic property in conventional reaction and reaction along with external electric field. As indicated in the electric field, the Fermi level increases and leads to increase in olefin yield. Zeolite band gap can be related to catalytic activity. The fermi level in the conventional reaction and reaction along with external electric field are presented in Table 2.

2.3. Process optimization

To obtain optimum operating parameters in oxidative dehydrogenation of LPG in an electric field, maximization of olefin yield, LPG conversion and selectivity were performed with central composite model. Table 4S in the Supplementary Material shows numerical optimum value for experimental parameters for olefin yield, LPG conversion and selectivity. The results indicated that the maximum value for LPG conversion (94.2%) can be resulted with temperature at 625.57 °C, input electrical current of 12 mA, gap distance of 9.70 mm and metal loading of 7.5wt.5. The results indicated that the maximum value for selectivity of 64.42% can be resulted with temperature at 697.20 °C, input electrical current of 3.30 mA, gap distance of 10.24 mm and metal loading of 3.98 wt.%. The results indicated that the maximum value for yield of 47.62% can be resulted with temperature at 673.66 °C, input electrical current of 11.01 mA, gap distance of 6.55 mm and metal loading of 3.98 wt.%. To validate the model some experiments were carried out over optimum value and experimental results for the LPG conversion, alkenes selectivity and yield were 93.29 %, 65.29%, and, 46.94%wt. respectively, that they were very close to the predicted value of the proposed model of central composite.

3. Materials and Methods

3.1. Catalyst preparation

Na-ZSM-5 was ion exchanged for 24 h through stirring with 1 M ammonium nitrate and 1 g zeolite/ 10 cm^3 solution at 80 °C in reflux treatment to achieve ammonium form of zeolite. Ammonium form was filtered with filter paper and vacuum pump. Then, it was washed with ionized water. Ion exchange was performed three times for each sample. Sample was dried

Preprints (www.preprints.org) | NOT PEER-REVIEWED | Posted: 21 May 2018 doi:10.20944/preprints201805.0268.v1

overnight at 110 °C and the sample was calcined at 823 K for 5 h under air flow to convert the ammonium ions to hydrogen form. The loading of chromium oxide with different weight fraction was carried out by impregnating of HZSM-5 with an aqueous solution of $Cr(NO_3)_3.9H_2O$ using the incipient wetness method. The weight fraction was in the range of 0.5-7.5 %wt. The impregnated samples were dried at 110 °C overnight for 12 h and then the samples were calcined under air flow, at 700 °C for 6 h.

3.2. Catalyst Characterization

The X-ray diffraction (XRD) patterns of different catalyst were determined in 5-80° (Cu Kα radiation, potential of generator (40 kV) and current of generator (30 mA). Hitachi S-4800 SEM was used to identify the morphology of each catalyst. Fourier Transform Infrared (FTIR) spectroscopy was employed to determine surface structure of catalyst. The specific surface areas of the samples were calculated by the Brunauer-Emmett-Teller (BET) method. The mesopore size distribution and total pore volumes were obtained using the Barrett-Joyner- Halenda (BJH) method. The optical band gap was measured with a UV–Vis spectrophotometer (Varian Cary 100). The optical absorption band was in the range of 200–1100 nm. The bang gap determined basis the Kubelka–Munk (K–M or F(R)) method (Equation 10):

$$F(R)=\frac{(1-R)^2}{2R} \tag{10}$$

Where, R is the reflectance percentage. The band gap of different catalyst can be determined by plotting F(R) versus energy in eV, and E_g was resulted by extrapolating slope of the graph [45]. Two ends of each catalyst were inserted at different temperatures in a thermally insulated reservoirs. The temperature is recorded by using thermocouples connected to a digital thermometer. Also, voltage difference measured by a voltmeter. It may require the warm water baths, cold-water baths, and dry ice-alcohol mixtures. Temperature differences between two ends of each catalyst should be less than 10 °C. Fermi level for p-type and n-type are calculated as follow:

$$\text{p-type semiconductor:} \quad TQ_pe=(Ef-Ev)+2kT \tag{11}$$

$$\text{n-type semiconductor:} \quad -TQ_ne=(Ec-Ev)+2kT \tag{12}$$

Where, E_F is Fermi level, E_v is the valence band energy, E_c is the conduction band energy, e is elementary electric charge, k is Boltzmann's constant, and T is average absolute (Kelvin) temperature of the sample, and Q is thermoelectric power which can be approximated for small differences of temperature [46].

$$Q=-\frac{dV}{dT}=-\frac{\Delta V}{\Delta T}=-\frac{\Delta V}{(T_2-T_1)} \tag{13}$$

Concentration of current carrier was obtained by measuring the Hall coefficient measurements at 25 °C with a PPMS system. Four-contact Hall-bar geometry was employed for the analyses. The carrier concentration determined from the $1/eR_H$ at 300 K, where e and R_H are the electric charge and hall coefficient, respectively [47]. Disk samples with a diameter of 10 mm diameter and thickness of 3 mm were prepared. Each catalyst was inserted between two copper circular disks. The impedance and phase angle were determined by changing the frequency with an impedance analyzer (Hewlett Packard model 4192A). The permittivity (ε') and loss factor (ε'') of complex dielectric constant were corresponded to the impedance Z and phase angle $\emptyset$ as

Preprints (www.preprints.org) | NOT PEER-REVIEWED | Posted: 21 May 2018 doi:10.20944/preprints201805.0268.v1

$$\varepsilon' = \frac{Z_i}{2\pi f C_0 Z^2} \quad (14)$$

$$\varepsilon'' = \frac{Z_f}{2\pi f C_0 Z^2} \quad (15)$$

Where, f, C_0 ($C_0=\varepsilon_0 A/T$), T, A, ε_0 are frequency, capacitance of electrod, thickness of disk and surface area of catalyst disck, and free space permitivity, respectively. Zi and Zr are imaginary and real part of the complex impedance which $Zi = Zsin\emptyset$ and $Zr = ZCos\emptyset$ [48].

3.3. Catalytic testing

100 mg of Cr/H-ZSM-5 catalyst was diluted with 50 mg of silica in the middle of the quartz reactor tube. Then, it was placed between two quartz wool. Initially, 40 ml per minute of air and then 25 ml per minute nitrogen were flown for 1 hour at 625 °C and passed across the catalyst. In the present study, LPG cylinder and CO_2 cylinder were used as feedstock and oxidant, respectively. The flow rates of LPG and carbon dioxide cylinders were controlled with a rotameter at 10 ml and 50 ml per minute, respectively. The gas mixture of 60 ml per minute at atmospheric pressure was diluted with balanced N_2 gas as a carrier gas. Cr/HZSM-5 catalysts were inserted into a fixed bed quartz reactor with a length of 124 cm and a diameter of 13 mm. The reaction temperature was controlled at various amounts of 550 °C to 700 °C. DC supply voltage was used to produce an external DC electric field in the catalyst bed. Change of electrical current was used to control the intensity of electric field. The alkanes, alkenes, CO_2, CO and other products were detected with Gas Chromatograph (GC) equipped with a 6 m Porapak Q packed column and a Flame Ionization Detector (FID). The gaseous products were analyzed on-line using a second GC equipped with a Thermal Conductivity Detector (TCD) and a carbon molecular sieve 601 column. Olefin yield, LPG conversion and selectivity were calculated using the following equations.

$$\text{Conversion of LPG} = \frac{\text{weight of LPG reacted}}{\text{weight of LPG initial}} \quad (16)$$

$$\text{Yield of light Olefin} = \text{The total wt.\% of ethylene and propylene} \quad (17)$$

$$\text{Selectivity of light Olefins} = \frac{\text{Yield of light Olefins}}{\text{Conversion of LPG}} \quad (18)$$

Figure S9 shows an experimental setup for the oxidative dehydrogenation of LPG in the external electric field.

3.4. Experimental design

A Central Composite Design (CCD) was used to achieve optimal conditions for four main parameters and interactions between these parameters. In this research, the main parameters were temperature, electrical current, gap distance and metal loading, shown with X_1–X_4, respectively. Temperature (X_1) range 550-700 °C, electrical current (X_2) range 0-12 mA, gap distance (X_3) range 6-14 mm and metal loading (X_4) range 0.5-7.5 wt.% were selected as presented in Table 3. Based on Central Composite Design (CCD), the number of experimental runs are calculated with Equation 19:

$$N = 2^k + 2k + x_0 \quad (19)$$

Preprints (www.preprints.org) | NOT PEER-REVIEWED | Posted: 21 May 2018 doi:10.20944/preprints201805.0268.v1

where N, k and x_0 are total experiments, main parameters and repetition of center point, respectively. The effects of each variable were investigated at five levels: -α, -1, 0, +1 and α, as shown in Table 3. The center point was investigated six times. So, 30 different combinations of random order experiments were carried out according to CCD for 4 parameters.

Table 3. Experimental level coded and range of independent parameters

Independent process parameter	-α	-1	0	+1	+α
Factor 1 (X_1): Temperature (C)	550.0	587.5	625.0	662.5	700.0
Factor 2 (X_2): B Electrical current (mA)	0	3	6	9	12
Factor 3 (X_3):C Gap distance (mm)	6	8	10	12	14
Factor 4 (X_4): D Metal loading (wt. %)	0.5	2.25	4	5.75	7.5

In order to investigate the interaction between the main factors, the second-order polynomial response equation was used. Also, this equation represents the relation between responses (yield, conversion and selectivity) to independent process parameters using Equation 20:

$$Y=\beta_0+\sum_{i=1}^{k}\beta_i x_i+\sum_{i=1}^{k}\beta_{ii}x_i^2+\sum_{i=1}^{k}\sum_{j=1}^{k}\beta_{ij}x_{ij}+\varepsilon \quad (20)$$

Where, Y is response as yield, conversion or selectivity, β_0 is constant that is intercept in ANOVA analysis, β_i, β_{ii} and β_{ij} are linear coefficient, quadratic coefficient and interaction coefficient, respectively, estimated for main factors, dual interaction and intraction between two factors, respectively. x_i is coded variable level, k is number of parameter and ε is a residual term [49, 50]. Using Design Expert software and Equation 20, coefficients of responses were calculated by the least squares method. To evaluate statistical significance of the model, ANOVA analysis, including R^2, adjusted R^2 and F-test was performed at the confidence level of 95%.

3.5. Statistical analysis

The ANOVA analysis of Central Composite Design (CCD) was used to specify significant terms among temperature (X_1), electrical current (X_2), gap distance (X_3) and metal loading (X_4), and significant second-order functions that fit experimental responses of conversion, yield and selectivity and the independent experimental variables, with the Design- Expert package version 7.3.0. F statistic was carried out to check the suitability of regression models. R-squared statistics were also investigated for the percentage variability of optimal parameters obtained by the model. To relate the response variables to main factors, surface and contour plots were used.

4. Conclusions

In oxidative dehydrogenation of LPG in an electric field, optimum operating parameters were obtained using central composite methodology. Operational variables were T(temperature), I(electrical current), GD(gap distance) and ML(metal loading). The experimental results analyzed with ANOVA. Temperature, electrical current and metal loading were the main variables that affect

yield and conversion and where temperature affects selectivity. Interaction between temperature and electrical current as well as electrical current and metal loading were the most interaction between two main factors. The predicted values obtained from the CCD model were adopted in accordance to the experimental results (R^2 = 0.96 for conversion, R^2 = 0.96 for selectivity and R^2=0.96 for yield). The band gap property of different catalyst can use as a criterion for study the performance of the catalyst. In the electric field applied to catalyst surface, surface charge on the catalyst surface is increased, energy band is curved and Fermi level is increased. Bending of energy band is a complex function of electric field and electronic properties of catalysts. As observed in experimental results, in the presence of higher metal loading and higher external electric field, due to synergetic effect, Fermi level is increased which is in favor to catalytic activity. The electric field which was applied on zeolite catalyst can be an effective method for increase in yield and conversion. The maximum olefin yield was 46.94% at 673.66 °C, 11.01 mA electric current, 6.55 mm gap distance and 3.98 wt. %. metal loading. Also, the maximum LPG conversion was 93.29% at 625.57 °C, 12 mA electric current, 9.7 mm gap distance and 7.5 wt.%. metal loading.

Supplementary Materials: The following are available online at www.mdpi.com/xxx/s1, Figure S1: title, Figure S1: title, Figure S1: The XRD patterns, Figure S2: SEM images, Figure S3: FTIR spectra, Figure S4: Comparison between experimental and predicted, Figure S5: perturbation curve, Figure S6: The response surface and contour plots as a function of the temperature and electrical current, Figure S7: The response surface and contour plots as a function of the electrical current and metal loading, Figure S8: The response surface and contour plots as a function of the electrical current and gap distance, Figure S9: Setup of the experiment, Table S1: Physicochemical properties, Table S2 ANOVA for response surface, Table S3: Coefficient of regression, Table S4: Obtained optimum values.

Author Contributions: In this paper, A.A. designed the experiments; A.A. performed the experiments; A.A. analyzed the data; the manuscript was written by A.A. and edited by R.K.

Funding: This research received no external funding.

Conflicts of Interest: The authors declare no conflict of interest.

References

1. Rovik, A.K.; Klitgaard, S.K.; Dahl, S.; Christensen, C.H.; Chorkendorff, I.; Effect of alloying on carbon formation during ethane dehydrogenation. *App. Cata. A: General*. **2009,** 358, 269-278.

2. Wu, J.; Sharada, S.M.; Ho, C.; Hauser, A.W.; Gordon, M.H.; Bell, A.T.; Ethane and propane dehydrogenation over PtIr/Mg(Al)O. *App. Cata. A: General*. **2015,** 506, 25-32.

3. Avila, A.M.; Yu, Z.; Fazli, S.; Sawada, J.A.; Kuznicki, S.M.; Hydrogen-selective natural mordenite in a membrane reactor for ethane dehydrogenation. *Micro and Meso Mat.* **2014,**190, 301-308.

4. Lisi, L.; Marchese, L.; Pastore, H.O.; Frache, A.; Ruoppolo, G.; Russo, G.; Evaluating the Catalytic Performances of SAPO-34 Catalysts for the Oxidative Dehydrogenation of Ethane. *Top Cata.* **2003,** 22, 95-99.

5. Gudgila, R.; Leclerc, C.A.; Support Effects on the Oxidative Dehydrogenation of Ethane to Ethylene over Platinum Catalyst. *Ind & Eng Chem Res.* **2011,** 50, 8438-8443.

6. Cavani, F.; Ballarini, N.; Cericola, A.; Oxidative dehydrogenation of ethane and propane: How far from commercial implementation?. *Cata Today.* **2007,** 127, 113-131.

7. Lobera, M.P.; Valer, S.; Serra, J.M.; Escolástico, S.; Argente, E.; Botti, V.; Optimization of ODHE membrane reactor based on mixed ionic electronic conductor using soft computing techniques. *Chem Eng Sci.* **2011,** 66, 6308-6317.

8. Sun, P.; Siddiqi, G.; Vining, W.C.; Chi, M.; Bell, A.T.; Novel Pt/Mg(In)(Al)O catalysts for ethane and propane dehydrogenation. *Cata.* **2011,** 282, 165-174.

9. Håkonsen, S.F.; Walmsley, J.C.; Holmen, A.; Ethene production by oxidative dehydrogenation of ethane at short contact times over Pt-Sn coated monoliths. *App Cata A: General.* **2010,** 378, 1-10.

10. Heracleous, E.; Lemonidou, A.A.; Ni–Me–O mixed metal oxides for the effective oxidative dehydrogenation of ethane to ethylene – Effect of promoting metal Me, *Cata.* **2010,** 270, 67-75.

11. Bañares, M.A.; Supported metal oxide and other catalysts for ethane conversion: a review. *Cata Today.* **1991**, 51, 319-348.

12. Nakagawa, K.; Kajita, C.; Ikenaga, N.; Suzuki, T.; Kobayashi, T.; Nishitani-Gamo, M.; Ando, T.; The Role of Chemisorbed Oxygen on Diamond Surfaces for the Dehydrogenation of Ethane in the Presence of Carbon Dioxide. *Phy. Chem. B.* **2003,** 107, 4048-4056.

13. Deng, Sh.; Li, S.; Li, H.; Zhang, Y.; Oxidative Dehydrogenation of Ethane to Ethylene with CO2 over Fe−Cr/ZrO_2 Catalysts. *Ind & Eng Chem Res.* **2009,** 48, 7561-7566.

14. Rodríguez, M.L.; Ardissone, D.E.; López, E.; Pedernera, M.N.; Borio, D.O.; Reactor Designs for Ethylene Production via Ethane Oxidative Dehydrogenation: Comparison of Performance. *Ind & Eng Chem Res.* **2011,** 50, 2690-2697.

15. Fierro, J.L.G.; Metal Oxides: Chemistry and Applications (Chemical Industries), CRC Press, 2005.

16. Solsona, B.; López Nieto, J.M.; Concepción, P.; Dejoza, A.; Ivars, F.; Vázquez, M.I.; Oxidative dehydrogenation of ethane over Ni–W–O mixed metal oxide catalysts. *Cata.* **2011,** 280, 28-39.

17. Solsona, B.; Concepción, P.; Hernández, S.; Demicol, B.; López Nieto, J.M.; Oxidative dehydrogenation of ethane over NiO–CeO2 mixed oxides catalysts. *Cata Today.* **2012,** 180, 51-58.

18. Cheng, Y.; Zhang, F.; Zhang, Y.; Miao, C.; Hua, W.; Yue, Y.; Gao, Z.; Oxidative dehydrogenation of ethane with CO_2 over Cr supported on submicron ZSM-5 zeolite. *Chi J Cata.* **2015,** 36, 1242–1248.

19. Zhang, F.; Wu, R.X.; Yue, Y.H.; Yang, W.M.; Gu, S.Y.; Miao, C.X.; Hua, W.M.; Gao Z.; Chromium oxide supported on ZSM-5 as a novel efficient catalyst for dehydrogenation of propane with CO_2. *Micro Meso Mater.* **2011,** 145, 194–199.

20. Wolkenstein, Th.; The Electronic Theory of Catalysis on Semiconductors. *Advances in Catalysis.* **1960,** 12, 189-264.

21. Deren, J.; Mania, R.; Effect of an external electric field on the oxidation of CO to CO_2 on a nickel oxide catalyst. *Catal.* **1974,** 35, 369-375.

22. Sekin, Y.; Tomioka, M.; Matsukata, M.; Kikuchi, E.; Catalytic degradation of ethanol in an electric field. *Cata Today.* **2009,** 146, 183–187.

23. Sekine, Y.; Haraguchi, M.; Matsukata, M.; Kikuchi, E.; Low temperature steam reforming of methane over metal catalyst supported on CexZr1−xO2 in an electric field. *Catalysis Today.* **2011,** 171, 116–125.

24. Oshima, K.; Tanaka K.; Yabe, T.; Kikuchi, E.; Sekine, Y.; Oxidative coupling of methane using carbon dioxide in an electric field over La–ZrO_2 catalyst at low external temperature. *Fuel.* **2013,** 107, 879–881.

25. Oshima, K.; Shinagawa, T.; Nogami, Y.; Manabe, R.; Ogo, Sh.; Sekine, Y.; Low temperature catalytic reverse water gas shift reaction assisted by an electric field. *Cata Today.* **2014,** 232, 27-32.

26. Oshima, K.; Shinagawa, T.; Haraguchi, M.; Sekine, Y.; Low temperature hydrogen production by catalytic steam reforming of methane in an electric field. *Int hydrogen energy.* **2013,** 38, 3003-3011.

27. Alamdari, A.; Karimzadeh, R.; Faradaic number as a criterion for the promotion effect of external electric field on the heterogeneous oxidative cracking of liquefied petroleum gas on ZSM-5 supported catalyst. *Reac Kinet Mech Cat.* **2018,** 123, 723-742.

28. Wang, H.; Xin, W.; Surface Acidity of H-Beta and Its Catalytic Activity for Alkylation of Benzene with Propylene. *Catal. Lett.* **2011,** 76, 225-229.

29Morrison, S.R.; Surface states associated with acid sites on solids. *Surf. Sci.* **1975,** 50, 329-342.

30. Tang, W.; Hu, Z.; Wang, M.; Stucky, G.D.; Metiu, H.; McFarland, E.W.; Methane complete and partial oxidation catalyzed by Pt-doped CeO_2. *J. Catal.* **2010,** 273, 125-137.

31. Ferreira, S.L.C.; Bruns, R.E.; Ferreira, H.S.; Matos, G.D.; Box-Behnken design: an alternative for the optimization of analytical methods. *Anal Chim Acta.* **2007,** 597, 179-186.

32. Zhang, X.; Wang, R.; Yang, X.; Yu, J.; Central composite experimental design applied to the catalytic aromatization of isophorone to 3,5-xylenol. *Chem. Inte. Lab. Sys.* **2007,** 89, 45–50.

33. K. M. Ralls, T. H. Courtney and J. Wulff: 'An introduction to materials science and engineering, 1st edn; 1976, New York, John Wiley and Sons.

34. Izci, E.; Izci, A. Dielectric Behavior of the Catalyst Zeolite NaY. *Turk J Chem* **2007,** 31, 523-530.

35. Chandrashekhar, G. V.; Cooper, E.; Shafer, M.W. Dielectric Properties of Macro-Defect-Free (MDF) Cements. *Mat. Sci.* **1989,** 24, 3356- 3360.

36. Franke, M.E.; Simon, U.; Proton mobility in H-ZSM5 studied by impedance spectroscopy. *Solid State Ionics.* **1999,** 118, 311-316.

37. Wang, Y.; Zhu, J.H.; Cao, J.M.; Chun, Y.; Xu, Q.H.; Basic catalytic behavior of MgO directly dispersed on zeolites by microwave irradiation. *Microporous and Mesoporous Materials.* **1998,** 26, 175-184.

38. Krylov, V. *Catalysis by Non-Metals*, Academic Press, New York, 1970.

39. Morris, B.; A dielectric study of the synthetic linde type-A zeolite-II. Dielectric properties of 5-A with adsorbed ammonia, sulphur dioxide, carbon dioxide and N-pentane. *J. Phys. Chem. Solids.* **1969,** 30, 89-101.

40. Rostovshchikova, T.N.; Smirnov, V.V.; Gurevich, S.A.; Kozhevin, V.M.; Yavsin, D.A.; Nevskaya, S.M.; Nikolaev, S.A.; Lokteva, E.S.; Nanostructured metal films: Fabrication and catalytic properties. *Catalysis Today*. **2005,** 105, 344-349.

41. Voskresenskaya, E.N.; Roguleva, V.G.; Anshits, A.G.; Catal. Oxidant Activation Over Structural Defects of Oxide Catalysts in Oxidative Methane Coupling. *Rev. Sci. Eng.* **1995,** 7, 101-143.

42. Grasselli, R.K.; Fundamental Principles of Selective Heterogeneous Oxidation Catalysis. *Top. Cata.* **2002,** 21, 79-88.

43. Jibril, B.Y.; Catalytic performances and correlations with metal oxide band gaps of metal-tungsten mixed oxide catalysts in propane oxydehydrogenation. *React. Kinet. Catal. Lett.* **2005,** 86, 171-177.

44. Pantazidis, A.; Bucholz, S.A.; Zanthoff, H.W.; Schuurman, Y.; Mirodatos, C.; Catalytic performance of $Al_2O_3/SiO_2/TiO_2$ loaded with V_2O_5 for the selective catalytic reduction of NO_x with ammonia. *Catalysis Today.* **1998,** 40, 207- 214.

45. Lopez, R.; Gomez, R.; Band-gap energy estimation from diffuse reflectance measurements on sol–gel and commercial TiO2: a comparative study. *Sol-Gel Sci. Tech.* **2012,** 61, 1-7.

46. Azároff, L. V.; Brophy, J. J. *Electronic processes in materials*, 1 st ed.; McGraw-Hill, Technology & Engineering, 1963.

47. Ananya, B.; Kanishka, B.; AgI alloying in SnTe boosts the thermoelectric performance via simultaneous valence band convergence and carrier concentration optimization. *Sol. Sta. Chem.* **2016,** 242, 43–49.

 doi:10.20944/preprints201805.0268.v1

615 48. El-Hadi, M. A.; Saqan, S.; Zihlif, A.; Ragosa, G.; Electrical impedance properties of zeolite composites. *Mat.*
616 *Tech.* **2008,** 23, 152-157.

617 49. Hassani, A.; Alidokht, L.; Khataee, A.R.; Karaca, S.; Optimization of comparative removal of two structurally
618 different basic dyes using coal as a low-cost and available adsorbent. *J. Taiwan Inst. Chem. Eng.* **2014,** 45, 1597–
619 1607.

620 50. Hassani, A.; Khataee, A.; Karaca, S.; Karaca, M.; Kıranşan, M.; Adsorption of two cationic textile dyes from
621 water with modified nanoclay: A comparative study by using central composite design. *Env Chem Eng.* **2015,** 3,
622 2738–2749.

623